



Cite this: *Mater. Adv.*, 2025,
6, 1191

Received 23rd September 2024,
Accepted 30th December 2024

DOI: 10.1039/d4ma00961d

rsc.li/materials-advances

Synthetic route for high-yield α'' -Fe₁₆N₂ submicron-sized powder using CaH₂ drying agent

Takayuki Tsuchida,^a Jun Fukushima,^a Masahiro Tobise^b and
Hirotugu Takizawa^a

The rare-earth-free magnetic material α'' -Fe₁₆N₂ is known to be a high-performance magnetic material. However, a synthetic route for high-yield α'' -Fe₁₆N₂ powder has not yet been established. In this study, a high-yield α'' -Fe₁₆N₂ submicron-sized powder was synthesized from Fe₃O₄ via H₂ reduction, and subsequent nitridation using a CaH₂ drying agent. Here, controlling the crystallite diameter of α -Fe is crucial to promoting nitridation. α -Fe powder with a crystallite diameter of approximately 20 nm was produced by lowering the reduction temperature and water vapor partial pressure. Thus, a high-yield α'' -Fe₁₆N₂ phase of 97 wt% could be obtained. Microstructural observations indicated that α'' -Fe₁₆N₂ submicron-sized powder with primary particles of 20–30 nm diameter could be synthesized. The α'' -Fe₁₆N₂ powder had much higher coercivity than that of the α -Fe powder. Thus, the process suggested in this study is expected to contribute to the development of applications of α'' -Fe₁₆N₂ in magnetic materials.

1. Introduction

Ferromagnetic materials have diverse applications, for example, in automotive motors and home appliances.^{1,2} Two main ferromagnetic materials used for practical applications include Nd–Fe–B and Ferrite magnets. Of these, the former is known to be the strongest magnet in the world.^{1–3} However, it is an expensive material, as it contains the rare-earth element Nd. The latter, *i.e.*, ferrite magnets are inexpensive, as they are rare-earth free; however, their magnetic performance is relatively low.^{1,2} Thus, a rare-earth-free magnet with a magnetic performance exceeding that of ferrite is desired. α'' -Fe₁₆N₂ meets the above-mentioned requirements and is expected to be a next-generation ferromagnetic material.⁴

Many studies related to α'' -Fe₁₆N₂ have been reported on thin films^{5–14} and nanoparticles,^{4,15–29} ever since the giant magnetic moment of α'' -Fe₁₆N₂ was discovered by Kim *et al.*⁵ For instance, Sugita *et al.* fabricated single-crystal α'' -Fe₁₆N₂ films by molecular beam epitaxy.⁶ Ogawa *et al.* synthesized single-phase α'' -Fe₁₆N₂ nanoparticles of approximately 100 nm by H₂ reduction and subsequent nitridation.⁴ However, the synthesis of α'' -Fe₁₆N₂ powder with a high bulk density is necessary for applications in ferromagnetic materials. Although there have been several reports on both powder^{30–33} and bulk³⁴ forms of α'' -Fe₁₆N₂, it contained some impurities, and its

production yield was low, thus hindering its use in any practical applications. Therefore, it has become necessary to establish a synthetic route to high-yield α'' -Fe₁₆N₂ powder for engineering applications.

Owing to the low diffusion rate of N atoms during NH₃ gas nitridation, powdering α'' -Fe₁₆N₂ was a challenge that needed to be tackled. One previous study suggested that the smaller the crystallite size of α -Fe nanoparticles, the higher the yield of α'' -Fe₁₆N₂ nanoparticles by nitridation.¹⁵ Thus, we focused on controlling the crystallite diameter of α -Fe during H₂ reduction of iron oxide powder. In general, the nucleation and growth of nuclei during H₂ reduction depends on the reduction temperature and water vapor partial pressure;³⁵ therefore, the crystallite diameter of the α -Fe powder can be reduced by controlling these parameters. Our previous study demonstrated that the partial pressure of water vapor was lowered by introducing a drying agent, such as the CaH₂ into the H₂ reduction system, and the reduction reaction from the Fe₃O₄ powder to α -Fe powder was lowered from 400 to 300 °C.³⁶ Therefore, in this study, synthesis of high-yield α'' -Fe₁₆N₂ submicron-sized powder was attempted *via* H₂ reduction and subsequent nitridation using a CaH₂ drying agent.

2. Materials and methods

A powder mixture sample (0.5 g) of Fe₃O₄ (Kojundo Chemical Lab. Co., 1 μ m pass) and CaH₂ (Sigma-Aldrich Co., LCC) was weighed in a 20:80 weight ratio. The amount of CaH₂ is sufficient to absorb H₂O, which is produced by the reduction

^a Department of Applied Chemistry, Graduate School of Engineering, Tohoku University, Sendai 980-8579, Japan. E-mail: takayuki.tsuchida.r3@dc.tohoku.ac.jp

^b Department of Electronic Engineering, Graduate School of Engineering, Tohoku University, Sendai 980-8579, Japan

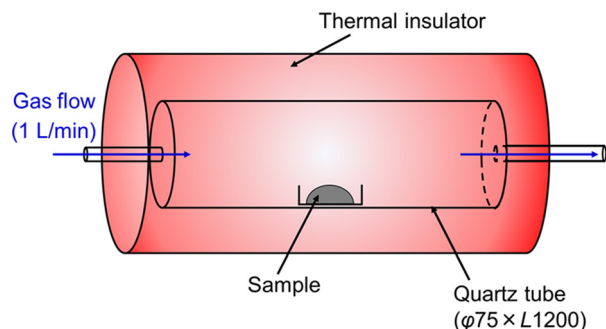


Fig. 1 Schematic diagram of the experimental setting.

reaction of Fe_3O_4 . This is effective in lowering the partial pressure of water vapor within the system, thereby promoting the reduction reaction. Both mixed and unmixed samples were investigated. Each of these samples was placed in a tube furnace, as shown in Fig. 1. H_2 reduction was conducted at two temperatures, namely 300 or 400 °C for 4 h under a 1 L min^{-1} H_2 gas flow. Subsequently, using an N_2 gas flow, the sample was cooled to ambient temperature. The sample was subsequently nitrided at a specific temperature in the range of 120–170 °C for 5 h under a 1 L min^{-1} ammonia gas flow. After the nitridation, the sample was cooled to ambient temperature, using the N_2 gas flow. The sample was then slowly oxidized by increasing the oxygen partial pressure in stages to atmospheric concentration before being removed from the tube furnace. The obtained sample was washed several times with a 0.1 M NH_4Cl (FUJIFILM Wako Pure Chemical Corporation) methanol solution and pure methanol to remove the by-products (CaO , $\text{Ca}(\text{OH})_2$, and CaH_2), and subsequently dried in vacuum. Next, a phase analysis of the sample was conducted using X-ray diffraction (XRD) with Co-K α source (Smart Lab, Rigaku); the microstructure of the samples was observed using transmission electron microscopy (TEM; EM-002B, TOPCON); and the magnetic properties of the samples were evaluated using superconducting quantum interference device (SQUID) measurements (MPMS, Quantum Design).

3. Results and discussion

3.1. Phase analysis of reduced samples

Fig. 2 shows the XRD profiles of the samples reduced under different conditions. The diffractions, under all the conditions, were assigned to α -Fe only, indicating that the reduction was complete as shown in chemical eqn (1). Table 1 shows the α -Fe crystallite diameter (D_{Fe}) values, calculated from the XRD profiles using Scherrer equation. First, the samples reduced at 400 °C with and without CaH_2 were compared. D_{Fe} of the sample reduced with CaH_2 was smaller than that of the sample reduced without CaH_2 . Next, the samples reduced with CaH_2 were compared. In this case, D_{Fe} of the sample reduced at 300 °C was smaller than that of the sample reduced at 400 °C. From the above it was concluded that α -Fe with a smaller D_{Fe} could be obtained using CaH_2 than with conventional H_2 reduction (*i.e.*, without a drying agent).

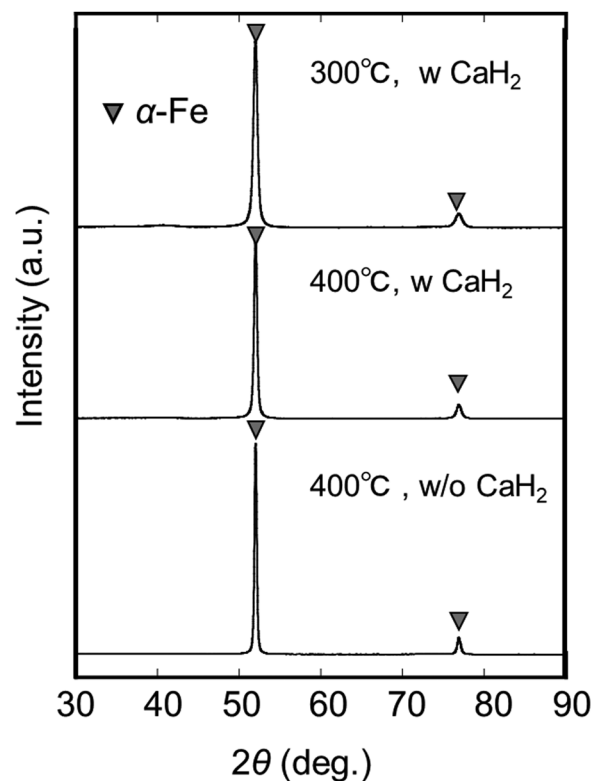
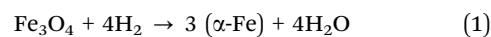


Fig. 2 XRD profiles of samples reduced under H_2 flow at two different temperatures with (w) and without (w/o) CaH_2 .

Table 1 D_{Fe} of samples reduced at two different temperatures with and without CaH_2

	400 °C w/o CaH_2	400 °C w CaH_2	300 °C w CaH_2
D_{Fe} (nm)	41.8	27.8	19.5



Next, the effect of the CaH_2 drying agent and reduction temperature on D_{Fe} will be discussed. For the samples reduced at 400 °C, D_{Fe} decreased in the presence of CaH_2 . Our previous study indicated that introducing the CaH_2 drying agent in the H_2 reduction system would lower the local partial pressure of water vapor in the iron oxide powder bed.³⁶ The decrease in the partial pressure of water vapor, accompanied by an increase in the partial pressure of H_2 , would contribute to an increase in the reaction rate and promotion of nucleation of α -Fe. Therefore, it is understood that a decrease in D_{Fe} in the presence of CaH_2 was owing to the promotion of α -Fe nucleation caused by a decrease in the partial pressure of water vapor. As regards the samples reduced with CaH_2 , D_{Fe} decreased upon lowering the reduction temperature from 400 to 300 °C. This might have been caused by the suppression of coarsening of the α -Fe crystallites. The mechanism described above is considered to be applicable to the reduction reactions of other oxides such as FeO and $\alpha\text{-Fe}_2\text{O}_3$ as well. This will be explored in future work.



3.2. Phase analysis of nitrided samples

Fig. 3(a) shows the XRD patterns of the samples reduced at 400 °C for 4 h and subsequently nitrided at 160–170 °C for 5 h without CaH_2 . Fig. 3(b) shows the production ratio of each phase calculated by reference intensity ratio (RIR) quantification. RIR quantification was performed using the software SmartLab Studio II (Rigaku), with PDF data for $\alpha''\text{-Fe}_{16}\text{N}_2$ referenced from no. 654562, $\alpha\text{-Fe}$ from no. 191830, $\gamma'\text{-Fe}_4\text{N}$ from No. 79980, and $\varepsilon\text{-Fe}_3\text{N}$ from No. 93190. The samples nitrided at 170 °C contained the $\gamma'\text{-Fe}_4\text{N}$ phase, whereas those nitrided at 160 °C did not contain the γ' phase. In addition, the samples nitrided at 170 °C contained more $\alpha\text{-Fe}$ phase than those nitrided at 160 °C. These results could be attributed to the decomposition of the $\alpha''\text{-Fe}_{16}\text{N}_2$ phase into $\alpha\text{-Fe}$ and $\gamma'\text{-Fe}_4\text{N}$ phases.³⁷ Consequently, 78 wt% of the maximum yield of the $\alpha''\text{-Fe}_{16}\text{N}_2$ phase was obtained from the nitridation of the samples reduced at 400 °C without CaH_2 .

Fig. 4(a) shows the XRD patterns of the samples reduced at 400 °C for 4 h and subsequently nitrided at 120–170 °C for 5 h with CaH_2 . Fig. 4(b) shows the production ratio of each phase as calculated by RIR quantification. The sample nitrided at 170 °C contained the γ' phase, as well as the ε phase (which is an excessively nitrided phase), whereas that nitrided at 160 °C did not contain the ε phase. Additionally, the sample nitrided at 150–170 °C contained the γ' phase, whereas that nitrided at 140 °C did not contain the γ' phase, but contained α'' and $\alpha\text{-Fe}$ phases. The lower the nitridation temperature, the lower the yield of the α'' phase in 120–140 °C range. As a result, 77 wt% of the maximum yield of the $\alpha''\text{-Fe}_{16}\text{N}_2$ phase was obtained from the nitridation of the samples reduced at 400 °C with CaH_2 .

Fig. 5(a) shows the XRD patterns of the samples reduced at 300 °C for 4 h, and subsequently nitrided at 130–170 °C for 5 h with CaH_2 . Fig. 5(b) shows the production ratio of each phase,

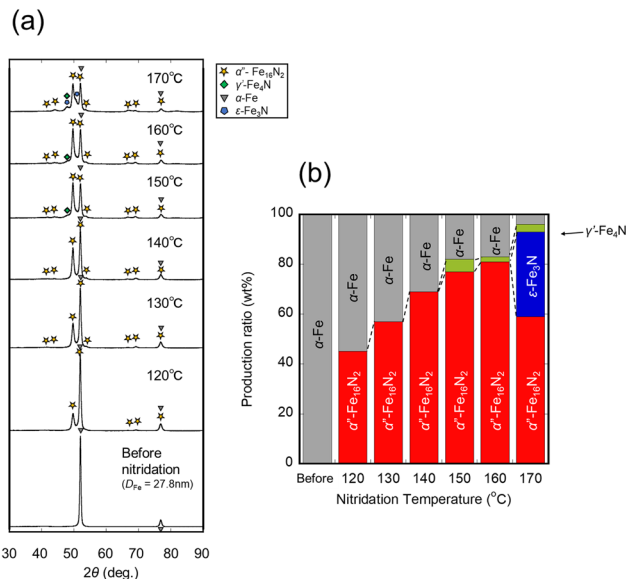


Fig. 4 (a) XRD profiles and (b) production ratio (wt%) of samples synthesized by H_2 reduction at 400 °C, and subsequently nitrided under NH_3 flow at different temperatures with CaH_2 .

as calculated by RIR quantification. The sample nitrided at 160–170 °C contained γ' and ε phases, whereas that nitrided at 150 °C did not contain any ε phase. Additionally, the sample nitrided at 150–160 °C contained the γ' phase, whereas that nitrided at 140 °C did not contain the γ' phase, but contained α'' and $\alpha\text{-Fe}$ phases. The lower the nitridation temperature, the lower the yield of the α'' phase in the range of 120–140 °C. As a result, 97wt% of the maximum yield of the $\alpha''\text{-Fe}_{16}\text{N}_2$ phase was obtained from the nitridation of the samples reduced at 300 °C with CaH_2 , which is more or less the α'' single phase.

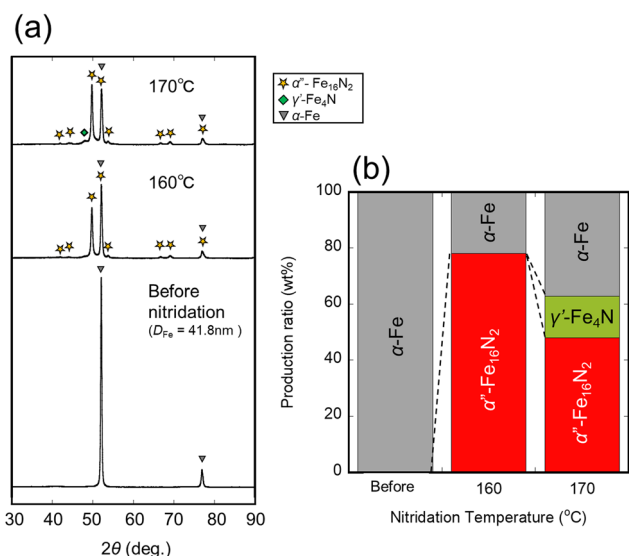


Fig. 3 (a) XRD profiles and (b) production ratio (wt%) of samples synthesized by H_2 reduction at 400 °C, and subsequently nitrided under NH_3 flow at different temperatures without CaH_2 .

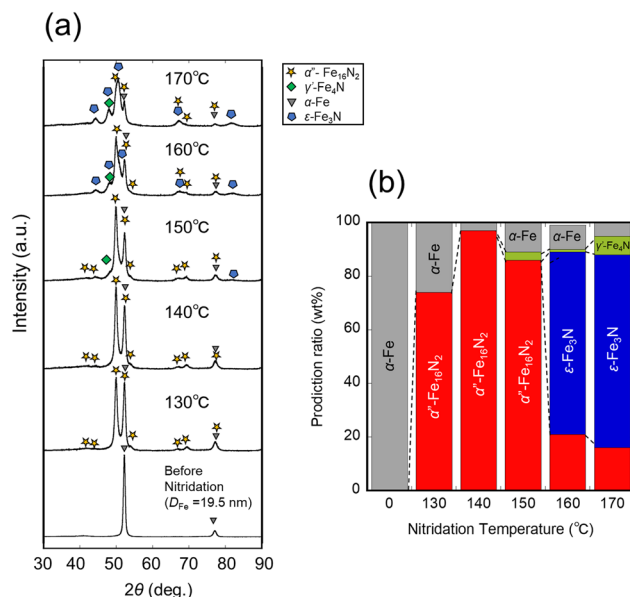


Fig. 5 (a) XRD profiles and (b) production ratio (wt%) of the samples synthesized by H_2 reduction at 300 °C, and subsequently nitrided under NH_3 flow at different temperatures with CaH_2 .

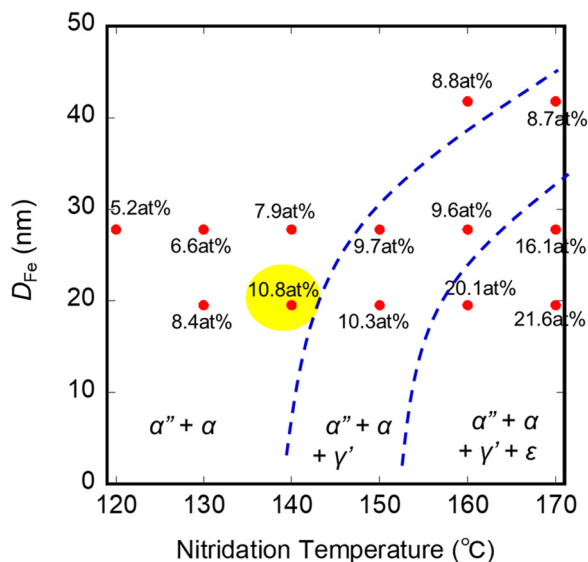
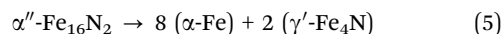
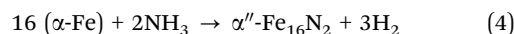
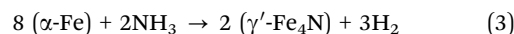
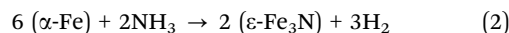


Fig. 6 Nitrogen content and formed phases as a function of nitridation temperature and D_{Fe} .

Fig. 6 shows a plot of the nitrogen content (at%) and the formed phase as a function of nitridation temperature and D_{Fe} , and reveals the effect of D_{Fe} on the phase formation of iron nitrides. It was observed that the nitrogen content increased, and the nitridation temperature at which an excessively nitrided phase was obtained (as shown in chemical eqn (2) and (3)) was lowered with a smaller D_{Fe} . It was inferred that the activation increased with an increase in the crystallite interface,

and the diffusion ability of nitrogen improved. As a result, a high-yield α'' phase was obtained by low-temperature nitridation (chemical eqn (4)), in which the decomposition of the α'' phase into α and γ' (chemical eqn (5)) phases could be prevented.



3.3. Microstructure

Next, the microstructure of the reduced and nitrided samples was observed to understand the change in microstructure after H_2 reduction and subsequent nitridation. Fig. 7 shows the TEM images of the raw powder; sample reduced at 300 °C for 4 h with CaH_2 ; and subsequently nitrided at 140 °C for 5 h with CaH_2 . The reduced sample was a submicron-sized powder with a nano-cluster structure comprising primary particles of 20–30 nm. The nitrided samples had almost the same structure. This result was consistent with the XRD measurements. Thus, submicron-sized $\alpha''\text{-Fe}_{16}\text{N}_2$ powder with a nano-cluster structure consisting of primary particles of 20–30 nm was successfully synthesized *via* H_2 reduction and subsequent nitridation using the CaH_2 drying agent.

3.4. Magnetic properties

Two critical magnetic performance properties, namely coercivity (H_c) and saturation magnetization (M_s) of the $\alpha''\text{-Fe}_{16}\text{N}_2$

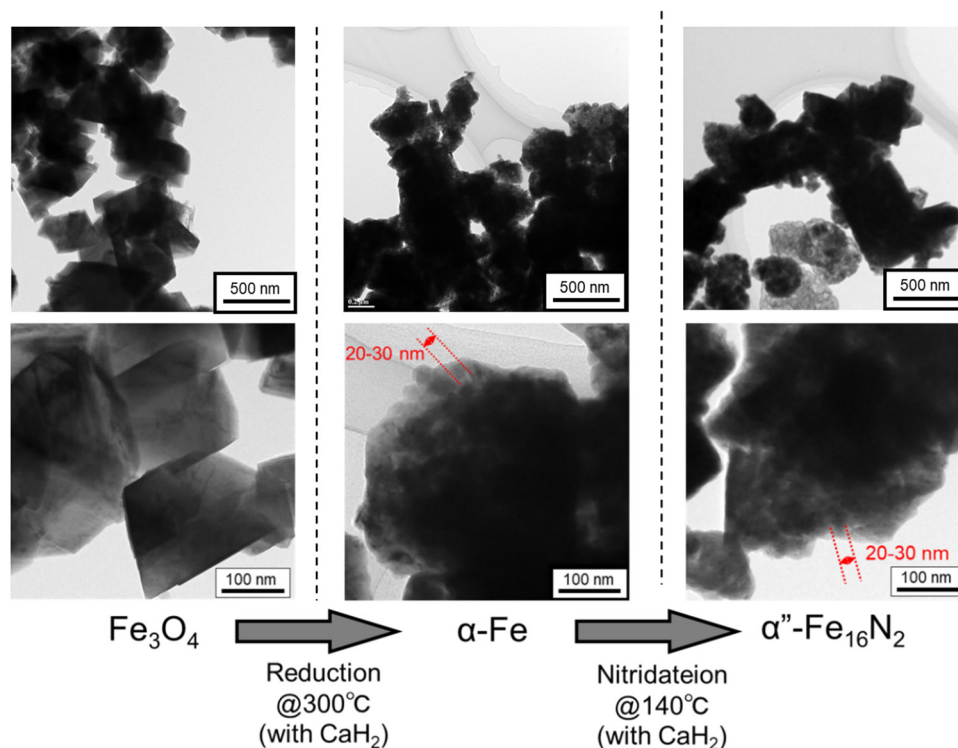


Fig. 7 TEM images of the raw material, reduced sample, and subsequently nitrided sample with CaH_2 drying agent.



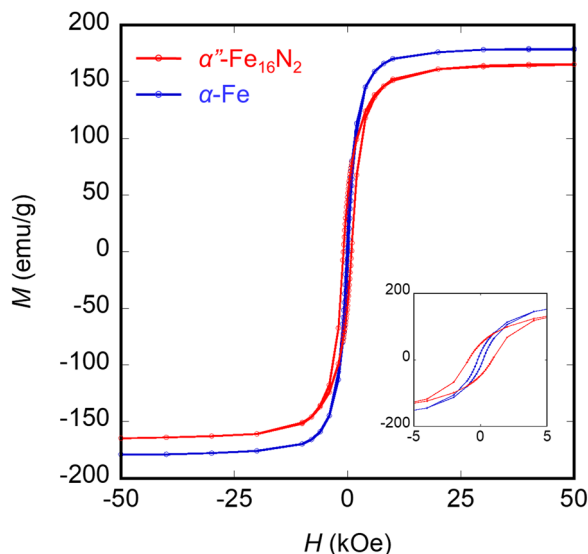


Fig. 8 M - H curve of the sample reduced at 300 °C with CaH_2 drying agent (α -Fe, blue plot), and sample reduced at 300 °C with CaH_2 drying agent and subsequently nitrated at 140 °C (α'' - Fe_{16}N_2 , red plot) measured at 300 K.

powders produced were analyzed. Fig. 8 shows the room temperature M - H curves of the sample reduced at 300 °C with CaH_2 (α -Fe powder), and sample reduced at 300 °C and nitrated at 140 °C with CaH_2 (α'' - Fe_{16}N_2 powder). Table 2 lists H_c and M_s of each sample. H_c of the α'' - Fe_{16}N_2 powder was 892 Oe at 300 K which was higher than that of the α -Fe powder (203 Oe). Moreover, the ratio of coercivity at 300 K to 10 K shows a higher value for α'' - Fe_{16}N_2 powder (~ 0.95) than that for α -Fe powder (~ 0.71). These suggest that the magnetic anisotropy $K_u V$ of α'' - Fe_{16}N_2 is strong against thermal fluctuations $k_B T$, which is considered evidence of the high magnetic anisotropy of α'' phase. Additionally, M_s of the α'' - Fe_{16}N_2 powder was slightly smaller than that of the α -Fe powder. Thus, α'' - Fe_{16}N_2 powder with high H_c and M_s could be synthesized *via* H_2 reduction and subsequent nitridation using the CaH_2 drying agent.

On the other hand, M_s of the α -Fe and α'' - Fe_{16}N_2 powders was much smaller than expected (222 emu g^{-1} for the theoretical value of α -Fe and 234 emu g^{-1} for nanoparticles of α'' - Fe_{16}N_2).^{4,38} In this study, the sample was slowly oxidized and exposed to air. Therefore, it was inferred that the small M_s value was owing to the oxide film formed during the oxidation

process. To further improve the magnetization, a process or an implementation that avoids oxidation is required.

4. Conclusion

In this study, a high-yield α'' - Fe_{16}N_2 submicron-sized powder, which is known to be a high-performance magnetic material, was synthesized *via* H_2 reduction and subsequent nitridation using CaH_2 as a drying agent. α -Fe powder with a small D_{Fe} of 19.5 nm was produced *via* H_2 reduction at 300 °C for 4 h in the presence of CaH_2 drying agent. α'' - Fe_{16}N_2 powder with a high yield of 97 wt% was successfully synthesized by nitridation of the α -Fe powder obtained as explained earlier at 140 °C for 5 h. From the microstructure observation, the α'' - Fe_{16}N_2 powder had a nano-cluster structure consisting of primary particles of 20–30 nm diameter. Magnetic property measurements indicated that the synthesized α'' - Fe_{16}N_2 powder had a high H_c of 892 Oe and M_s of 165 emu g^{-1} . The results of this study are significant for the application of α'' - Fe_{16}N_2 as a magnetic material and contribute to the development of the automotive and home appliance industries. Experimental validation as a permanent magnet is necessary and will be addressed in future work.

Data availability

All the data presented in this article are present in the form of figures and tables in the manuscript itself.

Conflicts of interest

There are no conflicts to declare.

Acknowledgements

This work was supported by the JSPS KAKENHI Grant-in-Aid for Scientific Research (S) Number JP19H05612. Magnetic measurements were performed at the Center for Low Temperature Science, Tohoku University. TEM measurements were performed at Institute for Materials Research, Tohoku University.

References

- 1 R. W. McCallum, L. Lewis, R. Skomski, M. J. Kramer and I. E. Anderson, Practical Aspects of Modern and Future Permanent Magnets, *Annu. Rev. Mater. Res.*, 2014, **44**, 451–477, DOI: [10.1146/annurev-matsci-070813-113457](https://doi.org/10.1146/annurev-matsci-070813-113457).
- 2 S. Hirokawa, M. Nishino and S. Miyashita, Perspectives for High-Performance Permanent Magnets: Applications, Coercivity, and New Materials, *Adv. Nat. Sci. Nanosci. Nanotechnol.*, 2017, **8**, 013002, DOI: [10.1088/2043-6254/aa597c](https://doi.org/10.1088/2043-6254/aa597c).
- 3 M. Sagawa, S. Fujimura, N. Togawa, H. Yamamoto and Y. Matsuura, New Material for Permanent Magnets on a Base of Nd and Fe (Invited, *J. Appl. Phys.*, 1984, **55**, 2083–2087, DOI: [10.1063/1.333572](https://doi.org/10.1063/1.333572).

Table 2 H_c and M_s of the sample reduced at 300 °C with CaH_2 drying agent (α -Fe), and sample reduced at 300 °C with CaH_2 drying agent and subsequently nitrated at 140 °C (α'' - Fe_{16}N_2); H_c and M_s were measured at 10 K and 300 K

	H_c (Oe)		M_s (emu g^{-1})	
	@10 K	@300 K	@10 K	@300 K
α'' - Fe_{16}N_2	937	892	175	165
α -Fe	284	203	182	178



- 4 T. Ogawa, Y. Ogata, R. Gallage, N. Kobayashi, N. Hayashi, Y. Kusano, S. Yamamoto, K. Kohara, M. Doi, M. Takano and M. Takahashi, Challenge to the Synthesis of α'' -Fe₁₆N₂ Compound Nanoparticle with High Saturation Magnetization for Rare Earth Free New Permanent Magnetic Material, *Appl. Phys. Express*, 2013, **6**, 14–17, DOI: [10.7567/APEX.6.073007](#).
- 5 T. K. Kim and M. Takahashi, New Magnetic Material Having Ultrahigh Magnetic Moment, *Appl. Phys. Lett.*, 1972, **20**, 492–494, DOI: [10.1063/1.1654030](#).
- 6 Y. Sugita, H. Takahashi, M. Komuro, K. Mitsuoka and A. Sakuma, Magnetic and Mössbauer Studies of Single-Crystal Fe₁₆N₂ and Fe–N Martensite Films Epitaxially Grown by Molecular Beam Epitaxy (Invited), *J. Appl. Phys.*, 1994, **76**, 6637–6641, DOI: [10.1063/1.358157](#).
- 7 Y. Sugita, H. Takahashi, M. Komuro, M. Igarashi, R. Imura and T. Kambe, Magnetic and Electrical Properties of Single-Phase, Single-Crystal Fe₁₆N₂ Films Epitaxially Grown by Molecular Beam Epitaxy (Invited), *J. Appl. Phys.*, 1998, **79**, 5576, DOI: [10.1063/1.362246](#).
- 8 P. Gupta, H. Fiedler, S. Rubanov and J. Kennedy, Magnetisation and Magnetic Anisotropy of Ion Beam Synthesised Iron Nitride, *J. Magn. Magn. Mater.*, 2021, **517**, 167388, DOI: [10.1016/j.jmmm.2020.167388](#).
- 9 J. P. Wang, N. Ji, X. Liu, Y. Xu, C. Sánchez-Hanke, Y. Wu, F. M. F. De Groot, L. F. Allard and E. Lara-Curzio, Fabrication of Fe₁₆N₂ Films by Sputtering Process and Experimental Investigation of Origin of Giant Saturation Magnetization in Fe₁₆N₂, *IEEE Trans. Magn.*, 2012, **48**, 1710–1717, DOI: [10.1109/TMAG.2011.2170156](#).
- 10 S. Higashikozono, K. Ito, F. Takata, T. Gushi, K. Toko and T. Suemasu, Highly Oriented Epitaxial ($\alpha'' + \alpha'$)-Fe₁₆N₂ Films on α -Fe(001) Buffered MgAl₂O₄(001) Substrates and Their Magnetization, *J. Cryst. Growth*, 2017, **468**, 691–695, DOI: [10.1016/j.jcrysgro.2016.11.048](#).
- 11 X. Hang, X. Zhang, B. Ma, V. Lauter and J. P. Wang, Epitaxial Fe₁₆N₂ Thin Film on Nonmagnetic Seed Layer, *Appl. Phys. Lett.*, 2018, **112**, 192402, DOI: [10.1063/1.5028396](#).
- 12 X. Zhang, Y. Jiang, M. Yang, L. F. Allard and J. P. Wang, High Ms Fe₁₆N₂ Thin Film with Ag under Layer on GaAs Substrate, *AIP Adv.*, 2016, **6**, 056203, DOI: [10.1063/1.4943236](#).
- 13 X. Zhang, V. Lauter, H. Ambaye and J. P. Wang, Thermal Stability of Fe₁₆N₂ Thin Film on GaAs (0 0 1) Substrate, *Mater. Res. Express*, 2017, **4**, 066401, DOI: [10.1088/2053-1591/aa72b3](#).
- 14 H. Y. Wang, E. Y. Jiang, H. L. Bai, Y. Wang, P. Wu and Y. G. Liu, The Effect of Ti Addition on the Thermal Stability of α'' -Fe₁₆N₂, *J. Phys. D: Appl. Phys.*, 1997, **30**, 2932–2935, DOI: [10.1088/0022-3727/30/21/005](#).
- 15 M. Tobise, S. Saito and M. Doi, Challenge to the Synthesis of α'' -(Fe, Co)₁₆N₂ Nanoparticles Obtained by Hydrogen Reduction and Subsequent Nitrogenation Starting from α -(Fe, Co)OOH, *AIP Adv.*, 2019, **9**, 035233, DOI: [10.1063/1.5079990](#).
- 16 J. Li, W. Yuan, X. Peng, Y. Yang, J. Xu, X. Wang, B. Hong, H. Jin, D. Jin and H. Ge, Synthesis of Fine α'' -Fe₁₆N₂ Powders by Low-Temperature Nitridation of α -Fe from Magnetite Nanoparticles, *AIP Adv.*, 2016, **6**, 125104, DOI: [10.1063/1.4967950](#).
- 17 K. Suzuki, A. Towata, Y. Kinemuchi, D. Nagai and M. Yasuoka, Preparation of Highly Dispersed Core-Shell α'' -Fe₁₆N₂/SiO₂ Particles Using Hydroxyapatite as a Sintering Prevention Layer, *J. Ceram. Soc. Jpn.*, 2017, **125**, 565–568, DOI: [10.2109/jcersj2.17037](#).
- 18 T. Ogi, Q. Li, S. Horie, A. Tameka, T. Iwaki and K. Okuyama, High-Purity Core-Shell α'' -Fe₁₆N₂/Al₂O₃ Nanoparticles Synthesized from α -Hematite for Rare-Earth-Free Magnet Applications, *Adv. Powder Technol.*, 2016, **27**, 2520–2525, DOI: [10.1016/j.appt.2016.09.017](#).
- 19 P. Palade, C. Plapcianu, I. Mercioniu, C. Comanescu, G. Schinteie, A. Leca and R. Vidu, Structural, Magnetic, and Mössbauer Investigation of Ordered Iron Nitride with Martensitic Structure Obtained from Amorphous Hematite Synthesized via the Microwave Route, *Ind. Eng. Chem. Res.*, 2017, **56**, 2958–2966, DOI: [10.1021/acs.iecr.6b04574](#).
- 20 C. W. Kartikowati, A. Suhendi, R. Zulhijah, T. Ogi, T. Iwaki and K. Okuyama, Effect of Magnetic Field Strength on the Alignment of α'' -Fe₁₆N₂ Nanoparticle Films, *Nanoscale*, 2016, **8**, 2648–2655, DOI: [10.1039/c5nr07859h](#).
- 21 M. Shibata, T. Ogawa and M. Kawashita, Synthesis of Iron Nitride Nanoparticles from Magnetite Nanoparticles of Different Sizes for Application to Magnetic Hyperthermia, *Ceram. Int.*, 2019, **45**, 23707–23714, DOI: [10.1016/j.ceramint.2019.08.086](#).
- 22 M. Tobise and S. Saito, Synthesis of α'' -(Fe,M)₁₆N₂ Nanoparticles Obtained by Hydrogen Reduction and Subsequent Nitridation Starting from α -(Fe,M)OOH (M = Co, Al), *IEEE Trans. Magn.*, 2022, **58**, 2100505, DOI: [10.1109/TMAG.2021.3084603](#).
- 23 I. Dirba, M. Mohammadi, F. Rhein, Q. Gong, M. Yi, B. X. Xu, M. Krispin and O. Gutfleisch, Synthesis and Magnetic Properties of Bulk α'' -Fe₁₆N₂/SrAl₂Fe₁₀O₁₉ Composite Magnets, *J. Magn. Magn. Mater.*, 2021, **518**, 167414, DOI: [10.1016/j.jmmm.2020.167414](#).
- 24 S. Kikkawa, A. Yamada, Y. Masubuchi and T. Takeda, Fine Fe₁₆N₂ Powder Prepared by Low-Temperature Nitridation, *Mater. Res. Bull.*, 2008, **43**, 3352–3357, DOI: [10.1016/j.materresbull.2008.02.008](#).
- 25 A. Suhendi, C. W. Kartikowati, R. Zulhijah, T. Ogi, T. Iwaki and K. Okuyama, Preparation and Characterization of Magnetic Films of Well-Dispersed Single Domain of Core-Shell α'' -Fe₁₆N₂/Al₂O₃ Nanoparticles, *Adv. Powder Technol.*, 2015, **26**, 1618–1623, DOI: [10.1016/j.appt.2015.09.005](#).
- 26 J. Li, W. Yuan, X. Peng, Y. Yang, J. Xu, X. Wang, B. Hong, H. Jin, D. Jin and H. Ge, Synthesis of Fine α -Fe₁₆N₂ Powders by Low-Temperature Nitridation of α -Fe from Magnetite Nanoparticles, *AIP Adv.*, 2016, **6**, 125104, DOI: [10.1063/1.4967950](#).
- 27 S. Yamashita, Y. Masubuchi, Y. Nakazawa, T. Okayama, M. Tsuchiya and S. Kikkawa, Crystal Structure and Magnetic Properties of “ α'' -Fe₁₆N₂” Containing Residual α -Fe Prepared by Low-Temperature Ammonia Nitridation”, *J. Solid*



- State Chem.*, 2012, **194**, 76–79, DOI: [10.1016/j.jssc.2012.07.025](https://doi.org/10.1016/j.jssc.2012.07.025).
- 28 I. Dirba, C. A. Schwöbel, L. V. B. Diop, M. Duerrschnabel, L. Molina-luna, K. Hofmann, P. Komissinskiy, H. Kleebe and O. Gutfleisch, Synthesis, Morphology, Thermal Stability and Magnetic Properties of α'' -Fe₁₆N₂ Nanoparticles Obtained by Hydrogen Reduction of γ -Fe₂O₃ and Subsequent Nitrogenation, *Acta Mater.*, 2017, **123**, 214–222, DOI: [10.1016/j.actamat.2016.10.061](https://doi.org/10.1016/j.actamat.2016.10.061).
 - 29 Y. Matsumoto, Y. Masubuchi, Y. Nakazawa, H. Itami, M. Tsuchiya and S. Kikkawa, Core Loss in Magnetic Rings Made of Fe₁₆N₂-like Iron Nitride Powder, *J. Alloys Compd.*, 2019, **789**, 697–703, DOI: [10.1016/j.jallcom.2019.03.061](https://doi.org/10.1016/j.jallcom.2019.03.061).
 - 30 J. Kim, J. Hwang and S. Yi, Iron Nitride Based Magnetic Powder Synthesized by Mechanical Alloying of Fe-Based Glassy Powders and Solid Nitrogen Compounds, *J. Magn. Mater.*, 2021, **539**, 168329, DOI: [10.1016/j.jmmm.2021.168329](https://doi.org/10.1016/j.jmmm.2021.168329).
 - 31 T. Saito, Production of Iron Nitrides by Mechanical Alloying, *J. Appl. Phys.*, 2000, **87**, 6514–6516, DOI: [10.1063/1.372755](https://doi.org/10.1063/1.372755).
 - 32 I. Paseka, P. Bezdička, A. Kláriková and K. Závěta, Structure and Magnetic Properties of Ball-Milled Iron Nitride Powders, *J. Alloys Compd.*, 1998, **274**, 248–253, DOI: [10.1016/S0925-8388\(98\)00536-2](https://doi.org/10.1016/S0925-8388(98)00536-2).
 - 33 O. Zirhli, N. Gunduz Akdogan, Y. N. Odeh, I. B. Misirlioglu, E. Devlin and O. Akdogan, Fabrication and Characterization of Fe₁₆N₂ Micro-Flake Powders and Their Extrusion-Based 3D Printing into Permanent Magnet Form, *Adv. Eng. Mater.*, 2020, **22**, 2000311, DOI: [10.1002/adem.202000311](https://doi.org/10.1002/adem.202000311).
 - 34 Y. Jiang, V. Dabade, L. F. Allard, E. Lara-Curzio, R. James and J. P. Wang, Synthesis of α'' -Fe₁₆N₂ Compound Anisotropic Magnet by the Strained-Wire Method, *Phys. Rev. Appl.*, 2016, **6**, 024013, DOI: [10.1103/PhysRevApplied.6.024013](https://doi.org/10.1103/PhysRevApplied.6.024013).
 - 35 M. Elzohiery, H. Y. Sohn and Y. Mohassab, Kinetics of Hydrogen Reduction of Magnetite Concentrate Particles in Solid State Relevant to Flash Ironmaking, *Steel Res. Int.*, 2017, **88**(2), 1600133, DOI: [10.1002/srin.201600133](https://doi.org/10.1002/srin.201600133).
 - 36 T. Tsuchida, J. Fukushima, M. Tobise, Y. Hayashi and H. Takizawa, Low-Temperature Hydrogen Reduction of Iron Oxide by Controlling the Water Potential Using a CaH₂ Drying Agent, *J. Solid State Chem.*, 2021, **302**, 122441, DOI: [10.1016/j.jssc.2021.122441](https://doi.org/10.1016/j.jssc.2021.122441).
 - 37 E. H. Du. Marchie van Voorthuysen, D. O. Boerma and N. C. Chechenin, Low-Temperature Extension of the Lehrer Diagram and the Iron-Nitrogen Phase Diagram, *Metall. Mater. Trans. A*, 2002, **33**, 2593–2598, DOI: [10.1007/s11661-002-0380-2](https://doi.org/10.1007/s11661-002-0380-2).
 - 38 K. Song, C.-Y. Suh, K.-S. Ko, J.-H. Bang, W. Kim and I.-J. Shon, The Effect of Phases in Nanoparticles Produced by Electrical Wire Explosion on Arsenic(III) Removal, *Mater. Trans.*, 2012, **53**, 739–744, DOI: [10.2320/matertrans.20111381](https://doi.org/10.2320/matertrans.20111381).

